Subproblem sampling vs. scenario reduction: Efficacy comparison for stochastic programs in power systems applications

Nahal Sakhavand[1] and Harsha Gangammanavar[2]

[1]Department of Industrial Manufacturing and Systems Engineering, University of Texas at Arlington, Arlington, TX-76010, USA

[2]Department of Engineering Management, Information, and Systems, Southern Methodist University, Dallas, TX-75275 USA

December 9, 2022

Abstract

In this paper, we present a two-stage stochastic programming and simulation-based framework for tackling large-scale planning and operational problems that arise in power systems with significant renewable generation. Traditional algorithms (the L-shaped method, for example) used to solve the sample average approximation of the true problem suffer from computational difficulties when the number of scenarios or the size of the subproblem increases. To address this, we develop a cutting plane method that uses sampling internally within optimization to select only a random subset of subproblems to solve in any iteration. We analyze the convergence property of the subproblem sampling-based method and demonstrate its computational advantages on two alternative formulations of the stochastic unit commitment-economic dispatch problem. We conduct the numerical experiments on modified IEEE-30 and IEEE-118 test systems. We also present detailed steps for assessing the quality of solutions obtained from sampling-based stochastic programming methods and determining a solution to prescribe to the system operators.

1 Introduction

Over the past couple of decades, there has been a significant increase in the share of energy generated from renewable resources in energy portfolios around the world. New capacity addition in renewable resources outpaced capacity addition in conventional energy resources by a factor of five [15]. These new capacity additions have largely been in solar and wind resources which are often classified together as intermittent energy resources. Their growth can be attributed not only to the environmentally friendly

characteristics but also to the fact that they have now become economically viable when compared to conventional resources like coal and nuclear [31].

However, a large-scale installation of renewable resources, particularly wind and solar, has brought forth the new challenges associated with operating the power grid. This is related to the two inherent characteristics of these resources *uncertainty* and *intermittency*. The stochasticity in renewable generation concerns with its dependence on environmental conditions such as temperature, humidity, cloud cover, etc. This makes predicting the amount of generation from these resources notoriously difficult. The intermittency on renewable resources, on the other hand, pertains to the inability to maintain continuous generation from these resources. It is also closely related to the large fluctuation in generation over short periods.

One of the principal power systems planning components is the Unit Commitment (UC) problem where the operating schedule for generators is determined. Several formulations and solution methodologies have been proposed for the UC problem that include dynamic programming and Mixed Integer Linear Programming (MILP). Another critical planning component is the Economic Dispatch (ED) problem where generation quantities of the scheduled generators are determined to ensure the balance between supply and demand. The ED problem is also formulated as an optimization problem (often as a linear program) that considers the topology of the power network. To the best of our knowledge, the current practice at system operators is to use a single point forecast of demand and renewable generation in the UC and ED problems. This results in deterministic instances of these optimization problems that can be solved using off-the-shelf deterministic solvers.

In order to accommodate the challenges introduced by integration of the renewable resources, new features such as increasing generation flexibility using fast-ramping operating reserves, demand-side management, and storage devices have been incorporated. In addition to these features, there has been a growing interest in migrating from deterministic optimization to more robust stochastic optimization tools to solve the UC and ED problems. While there are clear advantages of using stochastic optimization, their acceptance by power system operators is incumbent upon the availability of reliable algorithms that scale graciously to large-scale applications.

Decomposition-based stochastic programming (SP) models, particularly two-stage stochastic linear programs (2-SLP) with expectation-valued objective function, have proven to be very effective to model UC and ED problems. In these models, the first-stage corresponds to the decisions made before an observation of uncertainty and the second-stage allows for recourse actions that can be taken after the observation. Such a modeling approach provides a convenient tool to capture the complicated operational relationships such as minimum uptime/downtime requirements, nonlinear startup cost, etc. The first stochastic UC (S-UC) model is proposed in [35] which considers uncertainty in demand. In recent years, there have been a significant number of works that study S-UC with uncertainty in renewable generation such as wind and solar generation. We refer the interested reader to [38] for a comprehensive review of these works. Stochastic ED (S-ED) has been addressed using a deterministic equivalent form in [18], a probabilistic approach in [24], and a two-stage decomposition-based method in [8]. In several works (e.g., [2] and [34]), the UC problem is formulated as a first-stage program and the ED problem is included in the

second-stage to capture dispatch in response to observations of demand and renewable uncertainty. In SP models for UC and ED, it is critical to use an appropriate representation of the underlying uncertainty corresponding to renewable generation and demand. Such a representation is achieved by modeling them as continuous random variables. In this case, the computation of expectation-valued objective function involves multiple integrals, and therefore, approximate uncertainty representations must be employed. A popular approach is to consider a finite set of scenarios that are generated using Monte Carlo simulation approaches. The resulting optimization problem is referred to as the sample average approximation (SAA) problem [30]. This approach has been used for S-UC problems. For example, in [33] a sample of 10 scenarios and in [19] samples of sizes $\{50, 100, 200\}$ scenarios are used to set up the SAA. It is worthwhile to note that, once the sample is generated, the SAA problem is a deterministic optimization problem. In [33] and [19], the deterministic Benders decomposition is used as a solution procedure, albeit with a small number of scenarios.

The use of SAA is supported by strong theoretical backing. SAA is a consistent estimator of the original SP problem and exhibits an exponential rate of convergence (see Chapter 5 in [30] for detailed results). For problems involving discrete decision variables, which is the case in UC and ED problems, the asymptotic analysis of SAA was first conducted in [14]. While SAA provides asymptotic guarantees, the behavior of solutions obtained using a finite sample must be carefully assessed. Since a random sample is used to set up the SAA, the optimal value and the solution obtained by solving the SAA are stochastic. Therefore, a multiple replication-based approach is proposed in [20] which has been applied to assess the empirical behavior of SAA on several SP instances in [17]. Both the theoretical and empirical results indicate that increasing the number of samples used to generate the SAA will (i) reduce bias (the expected difference between the SAA and the true SP models' optimal values) and (ii) reduce variance across the replications. The two features can be viewed as certificates of quality and reliability of SP solutions, respectively. Unfortunately, using large sample sizes and multiple replication procedures can be computationally prohibitive for large-scale S-UC and S-ED problems.

A popular approach to address this computational difficulty is to employ *scenario reduction* techniques that reduce the original sample to a smaller subset of manageable size. These techniques are based on stability analysis of SP models and use probability metrics to identify "similar" scenarios and remove them from the original sample. In power systems applications, the use of the scenario reduction technique proposed by [5], particularly the faster variant developed by [10], is very common. This technique is based on the Kantorovich metric of probability distributions that takes into account the difference in the random vectors. For example, in [36] scenario reduction from 100 to 10 scenarios is used to compute commitment decisions and in [21] a sample of size 3018 is reduced to 20 to evaluate the economic value of the reserves. A scenario reduction technique that matches certain statistics (for e.g., moments) of the original and reduced scenario was proposed in [13] and adopted in a reserve requirement problem in [26]. The techniques discussed so far operate only in regards to the observations of the random vector and the associated probabilities are impervious to the decision problem. In other words, these scenario reduction techniques do not account for the impact of observations on the optimization outcome (optimal solution and value).

In [22], the authors use a similar approach to [5], but instead of using the difference in observations, they use the objective function value of the second-stage problem associated with the observations. A similar approach is used in [6] where observations are clustered based on the optimal objective function values, and then use the scenario reduction algorithm of [10] within each cluster. An importance sampling-based approach is used in [25] for selecting scenarios for the S-UC problem. In these approaches, computations necessary for scenario reduction/selection is performed at a particular first-stage decision variable (often the optimal solution of the mean-value problem). The decomposition-based SP methods generate a sequence of first-stage solutions which converge to the optimal solution. The efficacy of the reduced set is not necessarily the same across all solutions in the sequence, and hence, the scenario reduction techniques are mere heuristics without any solution quality guarantees on bias or variance.

In light of these observations, the main contribution of this paper are as follows:

a. We present a two-stage SP modeling and simulation framework for stochastic unit commitment-economic dispatch (S-UCED) that includes the UC problem in the first-stage and the ED problem in the second-stage. We consider two alternative formulations for the UC problem proposed in [23] and [1]. Our S-UCED model captures uncertainty in renewable generation whose scenarios are simulated using statistical time series models. An additional simulation feature is incorporated to enable efficient subproblem sampling (see (b.) below). This framework inherits the merit of SP models to outperform conventional models by providing more realistic solutions.

b. We present a cutting-plane SP algorithm with *subproblem sampling* designed specifically to solve S-UCED problems. There are two main advantages of the subproblem sampling-based approach. (i) It solves the original SAA problem to optimality in finite number of iterations. Thereby, retains the statistical properties of SAA such as a reduction in bias and variance with an increase in sample size. (ii) It significantly improves the computational performance over the SAA approach. In fact, its computational effort is comparable to what is required to solve the optimization problem obtained after scenario reduction.

c. We conduct comprehensive computational experiments to study the performance of our cutting-plane SP algorithm. We contrast the solutions obtained using our algorithms to those obtained by solving full sample SAA problems to assess the solution quality. We demonstrate the computational performance of our approach to the well-accepted scenario reduction technique using the fast-forward algorithm of [10]. The experiments are conducted on standard power systems instances from the literature.

While the focus of this paper is to solve the SAA of the S-UCED problem using randomization, sampling-based methods provide a viable practice to tackle various problems involving decision-making under uncertainty. The SAA-based approach has also been used to obtain approximate solutions for risk-averse [16] and chance-constrained [27] SP problems. Distributionally robust optimization provides a framework for data-driven settings with several attractive features, such as improved out-of-sample performance (compared to the SAA approach) and computationally viable solution approaches (for several commonly encountered structural features), see [28] for a detailed review. For risk-neutral problems,

instead of using a fixed representation of uncertainty as in SAA, the stochastic decomposition algorithm's sequential sampling approach allows one to dynamically determine the number of scenarios [11, 29].

The remainder of the paper is organized as follows. In Section 2, we present the S-UCED problem formulations used in this paper. Next, we proceed with the detailed subproblem sampling-based cutting-plane method in Section 3. We discuss the results of our computational experiments in Section 4, and finalize the paper with the conclusion in Section 5.

2 Problem Formulation

The principal idea of subproblem sampling-based cutting-plane method is suitable for general two-stage stochastic programs (2-SPs) which are applicable for a wide range of problems arising in power systems planning and operations. Due to the relative importance of the S-UCED problem, and the availability of standard test instances, we use this problem to illustrate the potential of our approach. When we have linear programs in both the stages, which is the case in the S-UCED problems, we can state the 2-SP in the following general form:

$$\begin{aligned} \min \;\; & f(\mathbf{x},\mathbf{z}) := c(\mathbf{x},\mathbf{z}) + \mathbb{E}\{Q(\mathbf{x},\mathbf{z},\tilde{\xi})\} && \text{(1a)} \\ \text{s.t } & (\mathbf{x},\mathbf{z}) \in \mathcal{X} := \{(\mathbf{x},\mathbf{z}) \mid A[\mathbf{x};\mathbf{z}] = b\} \subseteq \mathbb{R}^{n_1}_{+} \times \mathbb{B}^{m_1}, \end{aligned}$$

where $\mathbb{B} := \{0,1\}$. Here, the recourse function is the optimal value of the following program:

$$\begin{aligned} Q(\mathbf{x},\mathbf{z},\xi) = \min \;\; & d(\mathbf{y},\xi) && \text{(1b)} \\ \text{s.t } & W\mathbf{y} = r(\xi) - T[\mathbf{x};\mathbf{z}],\; \mathbf{y} \in \mathbb{R}^{n_2}_{+}. \end{aligned}$$

The first-stage decision $\mathbf{z}$ includes the binary commitment decisions and $\mathbf{x}$ captures the continuous decision variables in the UC problem. The second-stage program is solved for a given set of first-stage decisions $(\mathbf{x},\mathbf{z})$ and a realization ξ of the random vector $\tilde{\xi}$. We assume that the random vector is defined over the probability space $(\Xi,\mathcal{F},P)$, and is used to model uncertainty in demand and renewable generation over the horizon of the problem. The second-stage dispatch decisions are captured by the vector $\mathbf{y}$.

2.1 Unit Commitment

We consider two alternative formulations of the UC problem that were originally proposed in [23] and [1]. We refer to these formulations as MLR and ALS, respectively, after the initials of their corresponding authors. Our ED model is based on [8]. We study a two-stage multi-period S-UCED framework where uncertainty is due to the inclusion of renewable generation. In the following we only discuss the main differences between the two formulations and defer the detailed presentation to the online supplement.

Both the UC formulations use three binary variables to capture the status of a generator at any time period t. These decisions appear as vector $\mathbf{z}$ in (1a). In MLR, at any time period t, these binary variables take a value of 1 if (1) the generator is on, (2) the generator is turned on, and (3) the generator is turned off in time period t, respectively. On the other hand, in ALS, the first binary variable is defined as a

state-transition variable and is considered to be 1 if the unit *remains operational* and 0 otherwise. The use of state-transition variables, as opposed to the commitment decision variables in MLR, enables a network sub-structure in the UC problem formulation that provides certain computational advantages (see [1] and references therein for detailed discussions in the deterministic setting).

Both formulations capture the critical operational requirements of the UC problem. These include

- Minimum uptime and downtime requirement;
- Ramp-up/down and minimum start up/shut down generation requirements;
- Generation capacity restrictions; and
- Start-up costs that depend on the generators' idle time.

In the 2-SP setting of S-UCED, the UC decision is made before the realization of uncertainty. At this stage, requirements pertaining to transmission, power flows, etc. are often excluded. In turn, a system-wide requirement is included that mandates that the system-wide expected net-demand (expected demand minus expected renewable generation) is met by committed generation. In order to accommodate the possibility of deviating from the committed generation, once the actual demand and renewable generation is realized, supplementary generation or reserve capability needs to be committed. The MLR and ALS formulations capture these requirements differently. The MLR formulation addresses this requirement by including additional spinning reserve decision variables. The committed generation and the spinning reserve together constitute the continuous decision vector $\mathbf{x}$ in (1a). On the other hand, in the ALS the vector $\mathbf{x}$ comprises of the generation amount above the minimum capacity and maximum generation after adjusting for uncertainty (first introduced in [3]). The subtle differences in these alternative approaches to formulate the UC problem result in model instances that differ both in the computational performance as well as solution quality. We discuss these differences in our experimental study (§4).

2.2 Economic Dispatch

Once our commitment and reserve decisions are established in the first-stage, we determine the dispatch decisions that include actual generation, power flows, and phase angle for all time periods considered in the ED problem horizon. The formulation for the ED problem is adopted from [8]. These variables constitute the second-stage decision vector $\mathbf{y}$ in (1b). The hour-ahead generation cost represented in function $d(\cdot)$ is a piece-wise linear convex function of the dispatch amounts. The load shedding and generation curtailment penalties are also embedded in $d(\cdot)$. The constraints included in the ED problem include the following.

- The flow balance constraints which guarantees the conservation of energy at every bus in the network.
- Generation capacity restrictions and ramp-up/down requirements.

- Power flow equations. We use the DC linear approximation of the power flow that ignores reactive power and assumes second-order terms to be negligible.
- Bounds on bus phase angles, availability of renewable generation, and demand.

The stochastic elements in the ED problem correspond to demand and renewable generation. These terms appear on the right-hand side ($r(\xi)$) of the equality constraints in (1b). We refer the reader to the online supplement for the full model description.

3 Solution Method

Let us consider the SAA of (1) constructed using a sample $\Xi_n \subseteq \Xi$ of n demand and renewable generation scenarios. The first-stage objective can then be stated as

$$\min_{(\mathbf{x},\mathbf{z})\in\mathcal{X}} \; f_n(\mathbf{x},\mathbf{z}) := c(\mathbf{x},\mathbf{z}) + \frac{1}{N}\sum_{j=1}^{n} Q(\mathbf{x},\mathbf{z},\xi^j). \tag{2}$$

For problems with finite support, such as (2), the L-shaped method [32] has been very effective as a solution approach. In this method, a lower bounding approximation is constructed using a collection of affine functions (cuts). The computation of these affine functions involves solving the second-stage subproblem corresponding to all observations in Ξ_n to optimality, herein lies the computational bottleneck of the method. To alleviate this, we present the notion of subproblem sampling and introduce it within a cutting-plane method.

We begin by stating the assumptions on the SAA in (1).

(A1) For any UC feasible decision $(\mathbf{x},\mathbf{z})$ and observation $\xi \in \Xi_n$, there exists a feasible ED decision.

(A2) The dual feasible set of (1b) is non-empty.

(A3) The uncertainty only affects the right-hand side parameters in (1b).

Assumption (A1) is often referred to as the relatively complete recourse, which is satisfied by S-UCED if we allow for load-shedding and generation curtailment. Since the ED costs have a trivial lower bound of zero, assumption (A2) is satisfied. Finally, the demand and renewable generation affect only the right-hand side of the flow balance equations corresponding to the connected buses. Therefore, assumption (A3) is satisfied for S-UCED problems. This implies that the 2-SP model of S-UCED has a fixed recourse (i.e., matrix W is deterministic). Assumptions (A1) and (A2) together imply that the dual feasible set in bounded and the recourse value $-\infty < Q(\mathbf{x},\mathbf{z},\tilde{\xi}) < \infty$, for all $(\mathbf{x},\mathbf{z}) \in \mathcal{X}$ almost surely.

The dual of the ED problem in (1b) under assumptions (A1)–(A3) is given by

$$\begin{aligned} \max \; & \pi^\top (r(\xi) - T[\mathbf{x};\mathbf{z}]) \\ \text{s.t. } & \pi \in \Pi := \{\pi \mid W^\top \pi \le d'(\mathbf{y})\}. \end{aligned} \tag{3}$$

Notice that the dual feasible set is a polytope that is not affected by the randomness or the first-stage decision $(\mathbf{x},\mathbf{z})$. We denote the set of dual basic feasible solutions by Π. Linear programming duality ensures that any $\pi \in \Pi$ satisfies $Q(\mathbf{x},\mathbf{z},\xi) \ge \pi^\top(r(\xi) - T[\mathbf{x};\mathbf{z}])$ for all $(\mathbf{x},\mathbf{z}) \in \mathcal{X}$ and $\xi \in \Xi$. This observation motivates our subproblem sampling approach.

3.1 Subproblem Sampling-based Cutting-plane Method

We describe the steps of the algorithm in iteration k. At the beginning of the iteration, we have an approximation of the first-stage objective function $f_n^k(\mathbf{x}, \mathbf{z})$ defined using the set of affine functions $\mathcal{J}^{k-1}$, and a set of dual vertices discovered by the algorithm Π^{k-1}. The iteration begins by solving the master problem to identify a candidate solution:

$$(\mathbf{x}^k, \mathbf{z}^k) \in \arg\min \ \{c(\mathbf{x}, \mathbf{z}) + f_n^k(\mathbf{x}, \mathbf{z}) \mid (\mathbf{x}, \mathbf{z}) \in \mathcal{X}\}. \tag{4}$$

Let E^k denote a subset of observations obtained using Bernoulli sampling from the finite set Ξ_n. That is, every observation $\xi \in \Xi_n$ is subjected to an independent Bernoulli trial with a given probability $p \in [0, 1]$. For every $\xi \in E^k$, we set up and solve the subproblem $Q(\mathbf{x}^k, \mathbf{z}^k, \xi)$. The $\pi^k(\xi)$ denotes the optimal dual solution and is added to the collection of previously discovered dual vertices: $\Pi^k = \Pi^{k-1} \cup \{\pi^k(\xi)\}_{\xi \in E^k}$. For observation $\xi \in \Xi_n \setminus E^k$, the best dual vertex is identified from the collection Π^k using the "argmax" procedure

$$\pi^k(\xi) = \arg\max\{\pi^\top (r(\xi) - T(\xi)x^k | \pi \in \Pi^k\}. \tag{5}$$

The use of the argmax procedure above is inspired by its use in the SD algorithm [11]. In essence, for observations in the subset E^k an optimal dual solution is obtained by solving the subproblem to optimality and for those not included in the subset, the argmax procedure in (5) is employed to identify a suboptimal dual solution.

Using the set of dual solutions, we can then compute the affine function coefficients as follows:

$$\alpha^k = \pi^k(\xi^i)^\top r(\xi^i); \quad \beta^k = (-T(\xi^i))^\top \pi^k(\xi^i). \tag{6}$$

This affine function is added to the collection $\mathcal{J}^{k-1}$ to obtain $\mathcal{J}^k$. Using the latest affine function, the first-stage objective function is updated as follows:

$$f_n^k(\mathbf{x}, \mathbf{z}) = \max_{j \in \mathcal{J}^k} \ \{\alpha^j + (\beta^j)^\top [\mathbf{x}; \mathbf{z}]\}. \tag{7}$$

This completes one iteration of the algorithm. The complete algorithm is presented in Algorithm 1.

In the L-shaped method, subproblems associated with all the observations are solved in every iteration which can be achieved in Algorithm 1 by setting $p = 1$. In this sense, the subproblem sampling algorithm generalizes the standard L-shaped method. Further, since the subset E^k is a random sample, the coefficients in (6) are stochastic in nature. This marks a significant deviation from the deterministic coefficients generated in the L-shaped method which are deterministic.

The subproblem sampling-based cutting-plane method presented in Algorithm 1 is designed with an eye to improve the computational time while retaining optimality guarantees. The following proposition identifies the convergence of the algorithm.

Proposition 3.1. *Under assumptions (A1)–(A3), the subproblem sampling-based cutting-plane Algorithm 1 solves the problem in* (2) *in finite number of iterations.*

Algorithm 1 Subproblem sampling-based method

1: **Input:** $(\mathbf{x}^1, \mathbf{z}^1) \in \mathcal{X}$, sample set Ξ_n, and $\epsilon > 0$.
2: **Initialization:** Set $k \leftarrow 0$, $\mathcal{J}^k = \emptyset$, $\Pi^k = \emptyset$, $u^k = f_n(\mathbf{x}^1, \mathbf{z}^1)$, and $\ell^k = -\infty$.
3: **while** $(|u^k - \ell^k| > \epsilon)$ **do**
4: $k \leftarrow k + 1$.
5: Set up and solve the master problem in (4), and obtain candidate solution $(\mathbf{x}^k, \mathbf{z}^k)$ and optimal value ℓ^k.
6: Select $E^k \subseteq \Xi_n$,
7: **for** $\xi \in E^k$ **do**
8: Set up and solve the subproblem (1b) with $(\mathbf{x}^k, \mathbf{z}^k)$ and ξ as input and obtain optimal dual solutions $\pi^k(\xi)$.
9: Update $\Pi^k = \Pi^{k-1} \cup \{\pi^k(\xi)\}$.
10: **end for**
11: **for** $\xi \in \Xi_n \setminus E^k$ **do**
12: Pick $\pi^k(\xi)$ from Π^k using (5).
13: **end for**
14: Compute coefficients (α^k, β^k) using (6) and set $\mathcal{J}^k = \mathcal{J}^{k-1} \cup (\alpha^k, \beta^k)$.
15: Compute $u^k = \min\{u^{k-1}, \alpha^k + (\beta^k)^\top [\mathbf{x}^k; \mathbf{z}^k]\}$.
16: **end while**
17: **return** $(\mathbf{x}_n^*, \mathbf{z}_n^*) = (\mathbf{x}^k, \mathbf{z}^k)$ and $v_n^* = \ell^k$.

Proof. Notice that the dual vertex encountered in an iteration of the algorithm is used to update the set of dual vertices (Step 9. Therefore, the sequence of sets of dual vertices satisfies: $\Pi^{k-1} \subseteq \Pi^k \subseteq \Pi^{k+1}$, for all $k \geq 1$. Therefore, the first-stage objective function approximation in (7) satisfies:

$$f_n^{k-1}(\mathbf{x}, \mathbf{z}) \leq f_n^k(\mathbf{x}, \mathbf{z}) \leq f_n^{k+1}(\mathbf{x}, \mathbf{z})$$

for all $k \geq 1$. Moreover, since $\Pi^k \subseteq \Pi$ for all $k \geq 1$, we have $f_n^k \leq f_n$.

Since there are finitely many extreme points of the dual feasible region in (3), the number of affine functions with coefficients in (6) is also finite. Therefore, we have a $K < \infty$ such that $f_n^k(\mathbf{x}, \mathbf{z}) = f(\mathbf{x}, \mathbf{z})$ for all $k \geq K$. Thus, the solution $(\mathbf{x}^k, \mathbf{z}^k)$ do not change after iteration K.

When $f_n^k(\mathbf{x}^k, \mathbf{z}^k) = f(\mathbf{x}^k, \mathbf{z}^k)$, using the optimality of $(\mathbf{x}^k, \mathbf{z}^k)$ with respect to (4) we have

$$c(\mathbf{x}^k, \mathbf{z}^k) + f_n^k(\mathbf{x}^k, \mathbf{z}^k) \leq c(\mathbf{x}, \mathbf{z}) + f_n^k(\mathbf{x}, \mathbf{z}) \leq c(\mathbf{x}, \mathbf{z}) + f_n(\mathbf{x}, \mathbf{z}) \quad \forall (\mathbf{x}, \mathbf{z}) \in \mathcal{X}.$$

This implies that $(\mathbf{x}^k, \mathbf{z}^k)$ is optimal. Therefore, the algorithm must stop in finite number of iterations. □

Remark 1. The computational advantage offered by using subproblem sampling relies upon an efficient implementation of the argmax procedure in (5). Our implementation of the argmax procedure follows the steps in [12] tailored to the S-UCED problem. If the computational cost associated with the argmax procedure is higher than solving a subproblem to optimality, which is often the case for small-scale

problems, the classical L-shaped method will outperform the subproblem sampling method. However, when the subproblems are more involved like in the case of ED problems for large power systems, subproblem sampling is beneficial. Our computational experiments provide empirical evidence to support this claim.

Remark 2. Assumptions in (A1) and (A3) are included for ease of presentation, and can be relaxed with minimal additional effort. In the absence of complete recourse, we may encounter candidate solutions $(\mathbf{x}^k, \mathbf{z}^k)$ which may be infeasible for some observations in $\xi \in E^k$. This can be handled by generating feasibility cuts, similar to the L-shaped method. When the dispatch costs are random (see [36] and [37], for example), the dual feasible set is affected by randomness. Therefore, the argmax procedure must be carefully redesigned to account for randomness. This can be done based on the steps presented in [7]. Both these features have been included in our implementation of the algorithm.

3.2 Solution Quality Assessment

The solutions obtained by the procedure in Algorithm 1 are stochastic in nature due to the use of the random sample Ξ_n. Therefore, the solutions should not be accepted without posterior analyses.

From the SAA theory, we have $\mathbb{E}[v_n^*] \leq v^*$, where v_N^* and v^* are the optimal objective function values for the SAA problem and the true problem (1), respectively. In order to obtain an estimate of $\mathbb{E}[v_n^*]$, we adopt the multiple replication procedure presented in [20] to assess the quality of the solutions. Let M denote the number of replications. Let $(\mathbf{x}_n^{*,m}, \mathbf{z}_n^{*,m})$ and $v_n^{*,m}$ denote the optimal solution and value, respectively, obtained by solving the SAA with random sample Ξ_n^m. Using these the lower bound estimate and its variance can be calculated as

$$\mathcal{L}_n = \frac{1}{M}\sum_{m=1}^{M} v_n^{*,m};\ \sigma^2_{\mathcal{L}_n} = \frac{1}{(M-1)}\sum_{m=1}^{M}(v_n^{*,m} - \mathcal{L}_n). \tag{8}$$

To obtain an estimate of the upper bound, we note that $f(\mathbf{x}, \mathbf{z}) \geq v^*$ for any $(\mathbf{x}, \mathbf{z}) \in \mathcal{X}$. Using these we obtain an unbiased estimator of $f(\cdot)$ as

$$\mathcal{U}_{n'}^m = c(\mathbf{x}_n^{*,m}, \mathbf{z}_n^{*,m}) + \frac{1}{n'}\sum_{j=1}^{n'} Q(\mathbf{x}_n^{*,m}, \mathbf{z}_n^{*,m}, \xi^j). \tag{9}$$

Notice that the above estimator uses $n' \gg n$ realizations of the random vector that are simulated independently of the sample used for optimization. Using these estimates computed at solutions obtained from individual replication, an upper bound estimate can be computed as

$$\mathcal{U}_{n'} = \frac{1}{M}\sum_{m=1}^{M} \mathcal{U}_{n'}^m \tag{10}$$

Let $\sigma^2_{\mathcal{U}_{n'}}$ denote the variance of the above estimator. We can also compute the confidence intervals (CI) at level $(1-a)$ for the estimates in (8) and (10) as

$$\text{CI}_{\mathcal{L}} = \big[\mathcal{L}_n \pm \frac{\zeta_{a/2}\sigma_{\mathcal{L}}}{\sqrt{M}}\big];\quad \text{CI}_{\mathcal{U}} = \big[\mathcal{U}_{n'} \pm \frac{\zeta_{a/2}\sigma_{\mathcal{U}}}{\sqrt{M}}\big], \tag{11}$$

where $\zeta_{a/2}$ is the $(1-a/2)$ quantile of the standard normal distribution. Using the CIs computed above, we define a *pessimistic gap* as the difference between the upper limit of the $\text{CI}_{\mathcal{U}}$ and the lower limit of

$CI_{\mathcal{L}}$. If the pessimistic gap is lower than a desired threshold, then we have a statistical guarantee on the optimal objective function value.

4 Numerical Results

In this section, we present the numerical results from our experiments conducted on standard power systems test instances. To facilitate the discussion, we have identified the following questions of interest.

Q1. Does subproblem sampling alleviate the scale complexity of the algorithm and improve the computing time when compared to solving instances with the traditional L-shaped method (full sampling)?

Q2. How does subproblem sampling compare with the scenario reduction techniques that are prevalent in the application of sampling-based SP for power system problems?

Q3. What criteria do we need to follow in order to choose a solution for implementation among the set of optimal solutions obtained using the replicated process?

In addition to the above questions, we present a comparison between solutions recommended by the two different S-UCED formulations (MLR and ALS).

We conducted the experiments on modified IEEE-30 and IEEE-118 bus systems. Both these systems have been used extensively for research on planning and operations problems in the power systems, including UC, ED and operating reserve management (e.g., [9, 36]). The data for these systems are publicly available at [4]. Therefore, they serve as appropriate test systems for our numerical experiments. The modified IEEE-30 system has 30 buses along with 6 generators of which 2 of them are solar generators. The modified IEEE-118 bus system has 54 generators of which 36 are conventional and the remaining 18 are renewable generators. SAA instances were built for both MLR and ALS S-UCED formulations. These instances were used based on samples of independent and identically distributed scenarios of wind and solar generation of size $n = \{50, 100, 200, 500, 1000\}$. These scenarios were simulated in R using a time series model. The SAA instances were solved using the L-shaped method implemented on a *C/C++* platform using *CPLEX 12.9* on a Linux-based server with a processor of 64 GB RAM. The internal stopping criteria for the L-shaped method was set to $\epsilon = 0.01$ for the IEEE-30 bus system and $\epsilon = 0.05$ for the IEEE-118 bus system.

We conduct replicated experiments with $M = 30$. Across these 30 replications, we compute the lower bound estimate $\mathcal{L}_n$ and the out-of-sample upper bound estimate $\mathcal{U}_n$ using (8) and (10), respectively. We also compute the confidence intervals for $\mathcal{L}_n$ and $\mathcal{U}_n$ at $a = 5\%$ using (11). While presenting our results, we will present the lower bound and upper bound estimates along with the half-width of their confidence intervals. We also report the pessimistic gap and the average computational time with its standard deviation.

We report the results of the experiments conducted on the SAA instances in Table 1. These results were obtained using the L-shaped method with a two-hour upper limit on the computational time per replication. Recall that, in any iteration of the L-shaped method, one subproblem is solved for every scenario. Therefore, we refer to the results in Table 1 as "full sampling". Notice that the computational

Form.	Sample size (n)	Lower bound ($\mathcal{L}_n$) (95% CI)	Optimality gap (%)	Upper bound (95% CI)	Pessimistic gap	Avg. time (s) (std.dev.)
ieee30						
MLR	50	1234056.86 (± 3336.10)	[0.00,0.26]	1234332.36 (± 3218.20)	6829.80	0.16 (0.32)
	100	1251794.74 (± 1718.46)	[0.00,0.18]	1252343.25 (± 1618.45)	3885.42	0.29 (0.30)
	200	1234071.27 (± 3290.83)	[0.00,0.13]	1234332.36 (± 3218.20)	6770.13	0.46 (0.43)
	500	1262444.31 (± 780.46)	[0.00,0.10]	1262741.76 (± 694.83)	1772.74	7.30 (2.98)
	1000	1253194.94 (± 1546.53)	[0.00,0.06]	1253493.31 (± 1516.30)	3361.19	3.05 (4.50)
ALS	50	1266734.22 (± 861.30)	[0.00,0.99]	1269225.93 (± 1839.00)	5192.01	0.29 (0.20)
	100	1267082.10 (± 869.46)	[0.26,0.99]	1271369.52 (± 3765.83)	8922.71	0.54 (0.42)
	200	1266419.11 (± 478.18)	[0.01,0.89]	1267150.70 (± 979.26)	2189.03	0.89 (1.35)
	500	1269229.27 (± 1410.64)	[0.00,0.96]	1271640.43 (± 0.00)	3969.94	2.55 (4.93)
	1000	1265783.04 (± 308.91)	[0.00,0.70]	1268908.80 (± 100.54)	831.75	4.18 (11.36)
ieee118						
MLR	50	19045682.61 (± 17616.42)	[0.00,4.92]	19098268.00 (± 37376.28)	107578.10	190.11 (55.67)
	100	19009715.42 (± 12107.45)	[0.00,4.77]	19009243.53 (± 29409.36)	41044.93	244.36 (106.39)
	200	19021973.52 (± 16370.05)	[0.00,4.99]	19041180.70 (± 31289.23)	66866.47	573.30 (262.03)
	500	19021316.96 (± 24325.88)	[0.00,4.99]	19042827.98 (± 43434.77)	89271.67	981.09 (567.91)
	1000	19032001.64 (± 16217.00)	[0.00,4.97]	19070788.43 (± 32931.34)	87935.13	2512.34 (414.78)
ALS	50	20417256.35 (± 21082.2)2	[0.79,4.91]	20684425.88 (± 64392.12)	352643.88	332.21 (244.78)
	100	20394778.78 (± 19741.89)	[0.02,4.98]	20565529.61 (± 53848.69)	244341.40	722.93 (621.75)
	200	20406734.94 (± 22998.97)	[0.78,4.98]	20662373.52 (± 74182.92)	352820.47	1373.10 (1388.33)
	500	20414142.32 (± 24564.27)	[0.48,4.98]	20653011.92 (± 47164.43)	310598.30	2477.38 (1665.36)
	1000*	20542882.96 (± 19803.66)	[0.08,11.50]	20718775.93 (± 48102.20)	243798.83	3449.83 (2147.10)

Table 1: Results from L-shaped method applied to instances with full sampling.

time increases with the number of scenarios that can directly be attributed to the increased number of subproblem solves. Due to the large-scale nature of the IEEE-118 problem instances, the best solution achieved within the time limit is reported. For instance, the experiment with ALS for 1000 scenarios led to the termination of 4 replications due to the imposed time limit. The table also presents the range of optimization gaps at the termination of the optimization step. We use the term optimization gap to refer to the difference between lower and upper bounds, see $(u^k - \ell^k)$ in Algorithm 1. We will later define the optimality gap to refer to $f(\mathbf{x}, \mathbf{z}) - v^*$. SAA theory suggests that the variance of the lower bound estimate reduces with increasing sample size. However, we notice from the half-width of lower bound CI that it does not consistently decrease with increasing sample size. This can be ascribed to the fact that the problem instances are not solved to optimality in every replication, evident from the optimization gap column. In any case, the results in this table will serve as the basis of comparison in the remainder of this section.

Form.	p (Sample size, $\lvert E^k \rvert$)	Lower bound (95% CI)	Ratio	Avg. time (s) (std.dev.)	Improvement factor
`ieee30`					
MLR	0.05 (50)	1241682.00 (± 2617.33)	[0.98,0.99]	0.22 (0.30)	13.86
	0.10 (100)	1241904.79 (± 3134.71)	[0.98,1.00]	0.75 (1.32)	4.06
	0.20 (200)	1239342.42 (± 3100.47)	[0.98,1.00]	0.79 (1.20)	3.86
ALS	0.05 (50)	1272436.83 (± 987.74)	[0.99,1.01]	0.36 (0.61)	11.44
	0.10 (100)	1272280.08 (± 1250.31)	[0.99,1.01]	1.13 (1.37)	3.64
	0.20 (200)	1288524.33 (± 2250.78)	[1.00,1.02]	4.09 (4.40)	1.02
`ieee118`					
MLR	0.05 (50)	19024822.15 (± 10090.03)	[0.99,1.00]	52.75 (62.67)	47.62
	0.10 (100)	19049750.88 (± 13076.13)	[0.99,1.01]	142.55 (99.24)	17.62
	0.20 (200)	18978881.70 (± 14078.67)	[0.99,1.00]	318.11 (201.34)	7.90
ALS	0.05 (50)	20347358.79 (± 18616.66)	[0.98,1.00]	415.34 (270.99)	8.01
	0.10 (100)	20352103.65 (± 17239.45)	[0.99,1.00]	874.67 (134.03)	3.94
	0.20 (200)	20498263.58 (± 16103.20)	[0.99,1.00]	1226.06 (852.64)	2.81

Table 2: Subproblem sampling results for different values of probability p

4.1 Efficacy of Subproblem Sampling

In the L-shaped method, a significant portion of the computational time is spent in solving the subproblems. This time increases with the increase in the sample size n as well as the increase in the size of the subproblem. The subproblem sampling procedure presented in the Algorithm 1 is intended to address this issue. In order to verify the effect of subproblem sampling, we conducted the experiments on the same instances with sample size $n = 1000$ that were solved using full sampling. These results are presented in Table 2. By choosing the appropriate probability p, we allow a subset of subproblems to be solved in an iteration. The parenthetical values in the second column of the table shows the number of subproblems solved. Note that a random subset is selected in any iteration. We compute a ratio between the optimization objective function value obtained from the subproblem sampling procedure and the full sampling L-shaped method (with $n = 1000$). The range of these ratios is presented in this table. The table also includes the improvement factor in the computational time.

Notice that the subproblem sampling procedure recovers the optimal objective function value that is within 2% of the full sampling objective value. This attests to the fact that the quality of the solution obtained using subproblem sampling is statistically comparable to that obtained from full sampling. However, subproblem sampling significantly reduces the computational time. For example, for $|E^k| = 50$,

Form.	Sample size	σ_{Full}	Subproblem sampling		Scenario reduction		
			σ_{SS}	$\sigma_{SS}/\sigma_{Full}$	σ_{SR}	$\sigma_{SR}/\sigma_{Full}$	Time
`ieee30`							
MLR	50	3288.52	5565.48	1.69	16601.29	5.05	1.58 (0.42)
	100		6665.63	2.03	8900.32	2.71	2.63 (0.77)
	200		6592.81	2.00	11994.46	3.65	3.80 (1.27)
ALS	50	656.86	2760.30	4.20	7568.47	11.52	1.64 (0.58)
	100		3494.06	5.32	6652.50	10.13	2.29 (0.45)
	200		6289.93	9.58	6838.19	10.41	4.03 (1.86)
`ieee118`							
MLR	50	45319.29	28197.14	0.62	56932.20	1.26	74.60 (42.74)
	100		36541.96	0.81	35131.9	0.78	156.10 (91.52)
	200		39343.61	0.87	41972.30	0.93	339.28 (217.25)
ALS	50	55342.41	52025.26	0.94	64662.88	1.17	430.58 (485.10)
	100		48176.59	0.87	59808.06	1.08	657.94 (538.69)
	200		45001.27	0.81	53101.90	0.96	1233.32 (906.80)

Table 3: Comparison of subproblem sampling and scenario reduction results.

we observe that subproblem sampling reduces the computational time for solving the IEEE-30 instance by a factor of 13.86 in MLR. While the S-UCED serves as an excellent example of large-scale SP problems, we expect a similar computational advantage of subproblem sampling in any 2-SP. In particular, subproblem sampling can be used as an efficient alternative for SP problems encountered in power systems planning and operations.

4.2 Comparison with the Scenario Reduction Technique

Scenario reduction is often used when dealing with large-scale SP models for power systems planning and operations. The scenario reduction techniques are heuristic approaches to address the computational difficulties and do not provide any guarantees on solution quality (bias and variance reduction). Nonetheless, they provide a baseline for the subproblem sampling technique for computational comparison. For this comparison, we conducted an experiment in which we used the fast-forward scenario reduction technique from [10] to reduce a sample with $n = 1000$ to a smaller sample of size $n = \{50, 100, 200\}$. The results of this experiment are presented in Table 3. The table shows the standard deviation σ_{Full} of the lower bound estimate $\mathcal{L}_{1000}$ obtained from the full sampling L-shaped method. It also shows the standard deviations for subproblem sampling and scenario reduction with different n, σ_{SS} and σ_{SR}, respectively,

along with their ratios relative to σ_{Full}.

The results in Table 3 indicate that the solutions obtained from subproblem sampling have lower variability when compared to solutions obtained from scenario reduction. A solution with low variability provides the power system operator a greater confidence in what to expect if a solution is implemented. In terms of operations, a low variability solution implies lesser adjustments in the anticipative second-stage. The last column of the table shows the average computational time when scenario reduction is employed. This time includes the time of executing the fast-forward technique as well as optimization using the L-shaped method. Notice that the average time taking by subproblem sampling (see Table 2) is lower in all but one instance. Therefore, subproblem sampling not only provides a solution with low variability but also does so in computationally less time.

4.3 Identifying a Solution for Prescription

Since the SAA is constructed using a sample Ξ_n that is generated at random, the optimal objective function value v_n^* as well as the optimal solution $(\mathbf{x}_n^*, \mathbf{z}_n^*)$, are random functions of Ξ_n. Performing a single replication results in a single realization of these random functions. Moreover, the SAA theory suggests that the SAA optimal value is biased downwards, i.e., $\mathbb{E}[v_n^*] \leq v^*$ (see [30]). Therefore, the SAA optimal value underestimates (in expectation) the true optimal value. In order to assess the extent of the bias and the quality of the solution, performing the replicated experiments as presented in §3.2 is an essential step. Note that the replications can be carried out in parallel as they involve independent optimization and out-of-sample assessment steps.

The replicated experiments result in M different solutions which can be vastly different from one another. This is shown in Figure 1a where the pair-wise one-norm of commitment decisions ($|\mathbf{z}_n^{*,m} - \mathbf{z}_n^{*,m'}|$ for $m \neq m'$) is plotted for the IEEE-118 instance with sample size $n = 500$. The difference in the commitment decisions across all generators over the horizon of 24 hours was more than 300. For a given replication m, the objective function value $v_n^{*,m}$ can be viewed as a prediction of the total of unit commitment and expected dispatch costs. On the other hand, the out-of-sample value upper bound estimate can be viewed as validation. Figure 1b shows that in an overwhelming number of replications (28 out of 30) the optimization model underestimates the validation value, with a difference that is as high as 3.19%. This observation was consistent across all the instances used in our experiments.

The quality of the solution can be assessed using an independently generated sample resulting in an unbiased estimated of the upper bound $\mathcal{U}_{n'}^m$. The quality of the solution obtained in a replication can be assessed by calculating

$$G_n(\mathbf{x}_n^{*,m}, \mathbf{z}_n^{*,m}) = \mathcal{U}_{n'}^m - \mathcal{L}_n \qquad \forall m = 1, \ldots, M.$$

The first term is an unbiased estimate of $f(\mathbf{x}, \mathbf{z})$, the objective function value in (1a). The second term is an unbiased estimator for $\mathbb{E}[v_n^*]$. Since $\mathbb{E}[v_n^*] \leq v^*$, it serves as a lower bound estimate on the optimal objective function value v^*. This lower bound estimate is also shown in Figure 1b. Therefore, $G_n(\cdot)$ is an upper bound on the optimality gap $f(\mathbf{x}, \mathbf{z}) - v^*$. Figure 1c shows the gap attained at the solutions obtained from the 30 replications of the IEEE-118 instance with ALS formulation and a sample size

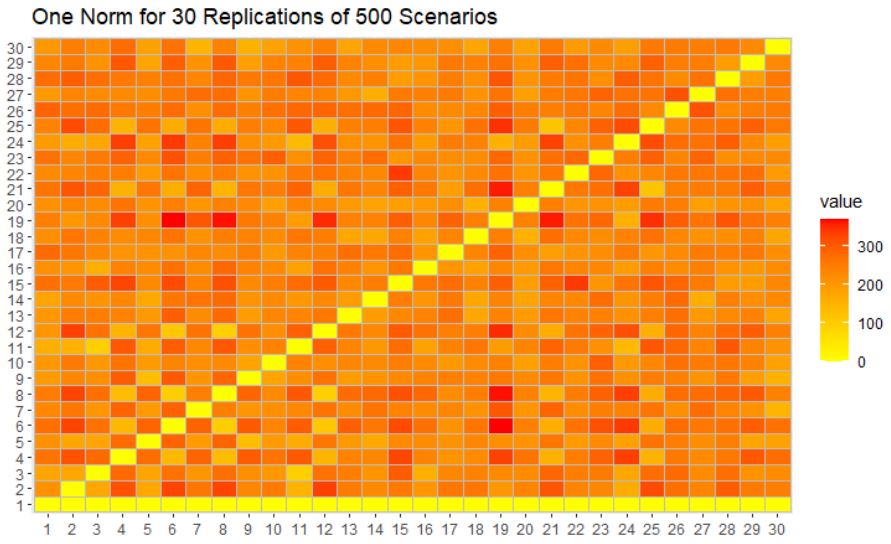

(a) One-norm difference between solutions

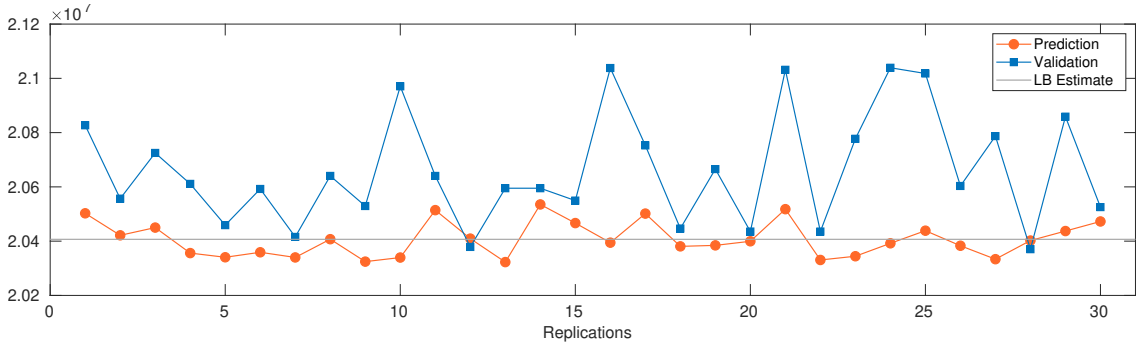

(b) Lower and upper bound estimates

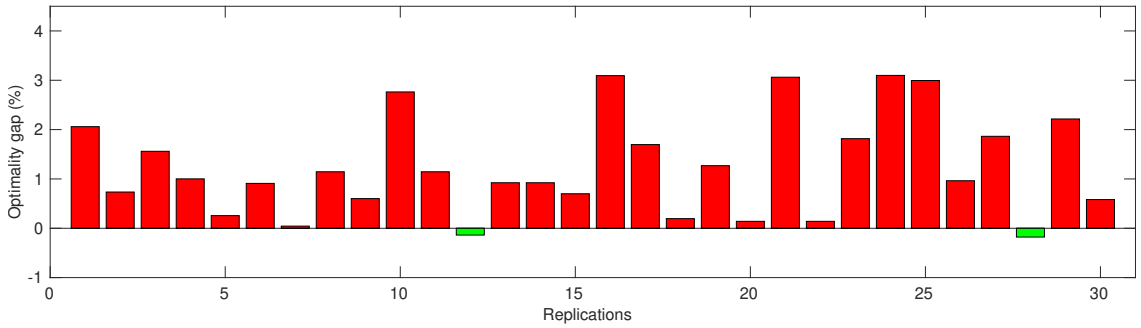

(c) Out-of-sample gap

Figure 1: Results for IEEE-118 ALS instance with $n = 500$.

$n = 500$.

Due to the inherent stochasticity, additional care must be taken when selecting a solution to prescribe among the pool of replicated solutions. We make the following observations about the solution pool $\{(\mathbf{x}_n^{*,m}, \mathbf{z}_n^{*,m})\}_{m=1}^{M}$ for the IEEE 118 instance with $n = 500$ that correspond to the results in Figure 4.3.

(C1) *Single replication solution,* $(\mathbf{x}_n^{*,1}, \mathbf{z}_n^{*,1})$*:* The optimization step predicted that the total commitment and dispatch cost is \$20.5 million. If the system operator implements this decision without

validation, then the system operator will incur a cost that is higher by as much as 1.6%.

(C2) *Solution with the smallest lower bound estimate:* After completing M replications, select μ such that $v^*_{n,\mu} \leq v^*_{n,m}$ for all $m = 1, \ldots, M$. The solution $(\mathbf{x}_n^{*,\mu}, \mathbf{z}_n^{*,\mu})$ corresponds to the one with the smallest lower bound. For the instance under consideration $\mu = 13$. If the system operator implements this solution, the total commitment and expected dispatch cost will be \$20.32 million. However, the validation results show that the total costs can be higher by at most 1.35% at \$20.59 million.

(C3) *Solution with the smallest upper bound estimate:* After completing the optimization and evaluation steps, identify the replication that yields a solution with the smallest upper bound. That is, select μ such that $\mathcal{U}^{\mu}_{n'} \leq \mathcal{U}^{m}_{n'}$ for all $m = 1, \ldots, M$. For the instance under study, the replication identified using the smallest upper bound criterion is $\mu = 28$ with a validation value of \$20.37 million.

(C4) *Solution with the smallest optimality gap:* Identify the replication index as

$$\mu \in \underset{m=1,\ldots,M}{\arg\min} \left\{ G_n(\mathbf{x}_n^{*,m}, \mathbf{z}_n^{*,m}) \right\}.$$

For the instance under consideration, $\mu = 28$. The solution identified using this criterion results in a validation value (\$20.37 million) that is lower than the prediction value (\$20.40 million).

For selecting an appropriate solution for prescription, the above criteria must be used in the reverse order. That is, the solution with the smallest out-of-sample gap estimate receives, that is criterion (C4), the highest preference for prescription. However, for large-scale S-UCED problems that cannot be solved to optimality, the solution with the smallest out-of-sample is not guaranteed to provide the smallest optimality gap. This is the case with the IEEE-118 instances as indicated by the large instance optimization gap column in Table 1. The criterion (C4) is applicable for IEEE-30 instances. For the IEEE-118 instance, a solution identified using (C3) is appropriate for prescription.

4.4 Comparison of Results from MLR and ALS Formulations.

We conclude our discussion on numerical results by comparing the solutions and the value associated with the MLR and ALS formulations of the S-UCED. Recall that in the MLR formulation, a separate variable is used to capture the capability of the generator to provide the spinning reserve. On the other hand, the ALS formulation models the maximum generation after adjusting for uncertainty. This maximum generation implicitly captures the reserve capability of the generator. This difference between the two formulations has a significant impact on the overall operating cost.

The results in Tables 1, 2 and 3 show that the overall cost corresponding to the ALS formulation is higher when compared to the cost associated with MLR formulation. This can be attributed to a higher amount of reserve requirement estimated by the ALS formulation. This can be seen in Figure 2. The histogram in Figure 2a shows the number of the generators providing a certain level of reserve capability and Figure 2b illustrates the average per generator over 24-hour horizon. In this sense, the ALS formulation is more conservative when compared to the MLR formulation. The ALS formulation is also computationally more expensive in comparison.

5 Conclusion

In this paper, we presented a stochastic optimization and simulation framework which utilizes two formulations of S-UCED with uncertainties in renewable generation. The resulting formulations are 2-SLPs with mixed-binary first-stage decisions and continuous recourse. We presented a sampling-based cutting plane method that solves only a subset of subproblems sampled in any iteration. This method is shown to converge in finitely many iterations. Moreover, the computational results conducted on a small-scale (IEEE-30) and a large-scale (IEEE-118) test systems reveal the computational advantage of subproblem sampling over the full sampling procedure of the L-shaped method. We also showed an improvement in computational performance over the scenario reduction technique. To tackle the inherent stochasticity of solutions obtained using sampling-based methods, we use a multiple replication procedure and devise rules to identify a high-quality solution among the pool of the solutions.

The cutting plane methods create approximations that are added to the master program as affine constraints in every iteration. As a consequence, the size of the master program increases with iterations

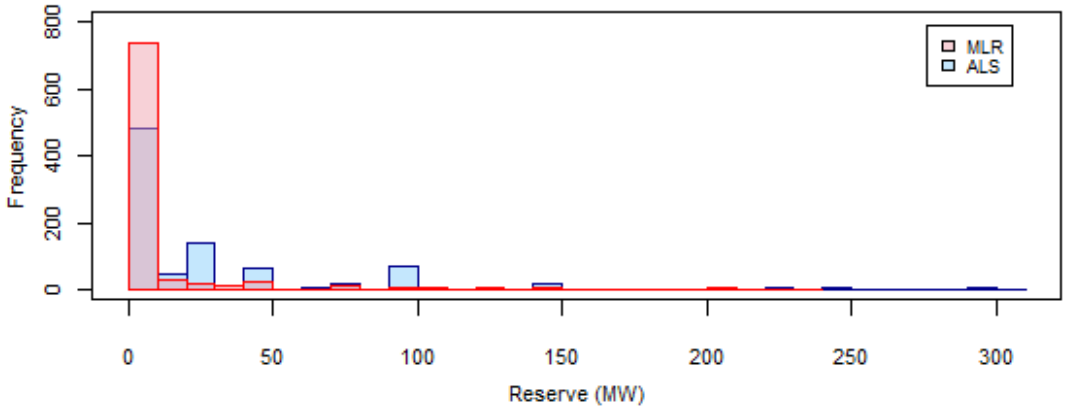

(a) Reserve frequency

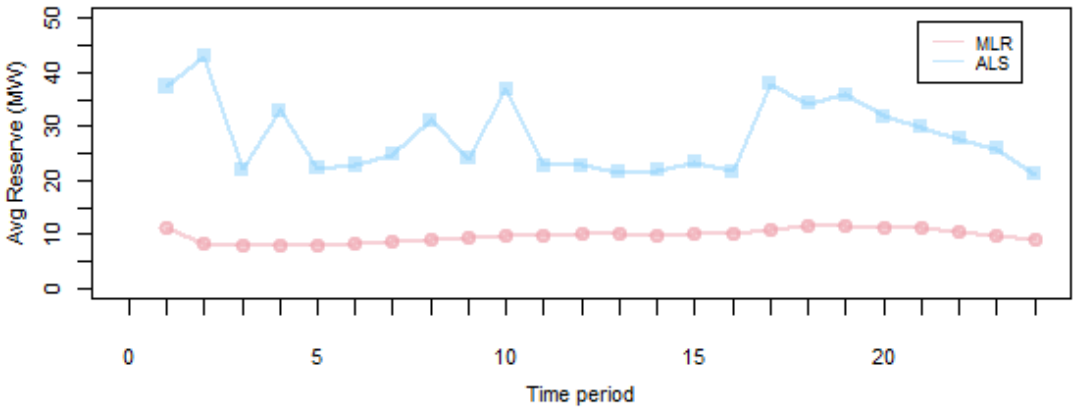

(b) Optimal reserve vs time

Figure 2: Estimation of the reserve requirement for IEEE-118 instance with $n = 1000$

and so does the time required to solve it. This was observed to be the case in our computational experiments. In order to address this, an alternative approach to approximate the expected recourse function in (1) can be established using the principles of the design and analysis of computer experiments (DACE) approach. We are currently developing such an algorithm and will report the results in our future work.

The subproblem sampling procedure works with a SAA of the the (1) that uses a finite number of observations. In our numerical study, each time the number of observations is increased, the optimization algorithm is restarted from scratch. Completing such an approach in a time-sensitive settings of power systems operations may prove to be challenging without high-performance computing resources. The sequential sampling algorithms, particularly the SD method [11], have proven to be effective in addressing this computational challenge. The current SD method does not support binary variables in the first-stage. We will undertake the development of the SD method customized to the S-UCED in our future research endeavor.

References

[1] Semih Atakan, Guglielmo Lulli, and Suvrajeet Sen. A state transition mip formulation for the unit commitment problem. *IEEE Transactions on Power Systems*, 33(1):736–748, 2017.

[2] Francois Bouffard and Francisco D Galiana. Stochastic security for operations planning with significant wind power generation. In *2008 IEEE Power and Energy Society General Meeting-Conversion and Delivery of Electrical Energy in the 21st Century*, pages 1–11. IEEE, 2008.

[3] Miguel Carrión and José M Arroyo. A computationally efficient mixed-integer linear formulation for the thermal unit commitment problem. *IEEE Transactions on power systems*, 21(3):1371–1378, 2006.

[4] Richard D. Christie. Power systems test case archive. Online: `http://www.ee.washington.edu/research/pstca/`, 08 1999. Accessed: 2015-08-01.

[5] J. Dupačová, N. Gröwe-Kuska, and W. Römisch. Scenario reduction in stochastic programming. *Mathematical Programming*, 95(3):493–511, 2003.

[6] Yonghan Feng and Sarah M. Ryan. Solution sensitivity-based scenario reduction for stochastic unit commitment. *Computational Management Science*, 13:29–62, 2016.

[7] Harsha Gangammanavar, Yifan Liu, and Suvrajeet Sen. Stochastic decomposition for two-stage stochastic linear programs with random cost coefficients. *INFORMS Journal on Computing*, 2020.

[8] Harsha Gangammanavar, Suvrajeet Sen, and Victor M Zavala. Stochastic optimization of sub-hourly economic dispatch with wind energy. *IEEE Transactions on Power Systems*, 31(2):949–959, 2015.

[9] Kory W Hedman, Richard P O'Neill, Emily Bartholomew Fisher, and Shmuel S Oren. Optimal transmission switching with contingency analysis. *IEEE Transactions on Power Systems*, 24(3):1577–1586, 2009.

[10] H. Heitsch and W. Romisch. Scenario reduction algorithms in stochastic programming. *Computational Optimization and Applications*, 24(2-3):187–206, 2003.

[11] J. L. Higle and S Sen. Stochastic decomposition: An algorithm for two-stage linear programs with recourse. *Mathematics of Operations Research*, 16(3):650–669, 1991.

[12] J. L. Higle and S Sen. *Stochastic Decomposition: A Statistical Method for Large Scale Stochastic Linear Programming*. Kluwer Academic Publishers, Boston, MA., 1996.

[13] Kjetil Høyland, Michal Kaut, and Stein W Wallace. A heuristic for moment-matching scenario generation. *Computational optimization and applications*, 24(2-3):169–185, 2003.

[14] Anton J Kleywegt, Alexander Shapiro, and Tito Homem-de Mello. The sample average approximation method for stochastic discrete optimization. *SIAM Journal on Optimization*, 12(2):479–502, 2002.

[15] Sam Koebrich, Thomas Bowen, and Austen Sharpe. *2018 Renewable Energy Data Book*, 2018.

[16] Václav Kozmík and David P. Morton. Evaluating policies in risk-averse multi-stage stochastic programming. *Mathematical Programming*, 152(1):275–300, Aug 2015.

[17] J. Linderoth, A. Shapiro, and S. Wright. The empirical behavior of sampling methods for stochastic programming. *Annals of Operations Research*, 142(1):215–241, 2006.

[18] K Liu and J Zhong. Generation dispatch considering wind energy and system reliability. In *IEEE PES General Meeting*, pages 1–7, 2010.

[19] Yang Liu and Nirmal-Kumar C Nair. A two-stage stochastic dynamic economic dispatch model considering wind uncertainty. *IEEE Transactions on Sustainable Energy*, 7(2):819–829, 2015.

[20] Wai-Kei Mak, David P Morton, and R Kevin Wood. Monte carlo bounding techniques for determining solution quality in stochastic programs. *Operations research letters*, 24(1-2):47–56, 1999.

[21] J. M. Morales, A. J. Conejo, and J. Perez-Ruiz. Economic valuation of reserves in power systems with high penetration of wind power. *IEEE Transactions on Power Systems*, 24(2):900–910, 2009.

[22] J. M. Morales, S. Pineda, A. J. Conejo, and M. Carrion. Scenario reduction for futures market trading in electricity markets. *IEEE Transactions on Power Systems*, 24(2):878–888, 2009.

[23] Germán Morales-España, Jesus M Latorre, and Andres Ramos. Tight and compact milp formulation for the thermal unit commitment problem. *IEEE Transactions on Power Systems*, 28(4):4897–4908, 2013.

[24] GJ Osório, JM Lujano-Rojas, JCO Matias, and JPS Catalão. A probabilistic approach to solve the economic dispatch problem with intermittent renewable energy sources. *Energy*, 82:949–959, 2015.

[25] A Papavasiliou and S.S. Oren. Multiarea stochastic unit commitment for high wind penetration in a transmission constrained network. *Operations Research*, 61(3):578–592, 2013.

[26] A Papavasiliou, S.S. Oren, and R.P. O'Neill. Reserve requirements for wind power integration: A scenario-based stochastic programming framework. *IEEE Transactions on Power Systems*, 26(4):2197–2206, Nov 2011.

[27] Alejandra Peña Ordieres, James R Luedtke, and Andreas Wächter. Solving chance-constrained problems via a smooth sample-based nonlinear approximation. *SIAM Journal on Optimization*, 30(3):2221–2250, 2020.

[28] Hamed Rahimian and Sanjay Mehrotra. Distributionally robust optimization: A review. *arXiv preprint arXiv:1908.05659*, 2019.

[29] S. Sen and Y. Liu. Mitigating uncertainty via compromise decisions in two-stage stochastic linear programming: Variance reduction. *Operations Research*, 64(6):1422–1437, 2016.

[30] A. Shapiro, D. Dentcheva, and A. Ruszczynski. *Lectures on Stochastic Programming: Modeling and Theory, Second Edition*. Society for Industrial and Applied Mathematics, Philadelphia, PA, USA, 2014.

[31] U.S. Energy Information Administration. *Annual Energy Outlook 2020 with projections to 2050*, 2020.

[32] Richard M Van Slyke and Roger Wets. L-shaped linear programs with applications to optimal control and stochastic programming. *SIAM Journal on Applied Mathematics*, 17(4):638–663, 1969.

[33] Jiadong Wang, Jianhui Wang, Cong Liu, and Juan P Ruiz. Stochastic unit commitment with sub-hourly dispatch constraints. *Applied energy*, 105:418–422, 2013.

[34] Jianhui Wang, Audun Botterud, Vladimiro Miranda, Cláudio Monteiro, and Gerald Sheble. Impact of wind power forecasting on unit commitment and dispatch. In *Proc. 8th Int. Workshop Large-Scale Integration of Wind Power into Power Systems*, pages 1–8, 2009.

[35] Rolf Wiebking. Stochastische modelle zur optimalen lastverteilung in einem kraftwerksverbund. *Zeitschrift für Operations Research*, 21(6):B197–B217, 1977.

[36] Lei Wu, Mohammad Shahidehpour, and Tao Li. Stochastic security-constrained unit commitment. *IEEE Transactions on power systems*, 22(2):800–811, 2007.

[37] Bining Zhao, Antonio J Conejo, and Ramteen Sioshansi. Unit commitment under gas-supply uncertainty and gas-price variability. *IEEE Transactions on Power Systems*, 32(3):2394–2405, 2016.

[38] Qipeng P Zheng, Jianhui Wang, and Andrew L Liu. Stochastic optimization for unit commitment—a review. *IEEE Transactions on Power Systems*, 30(4):1913–1924, 2014.